BIOMATERIALS SYNTHESIS AND CHARACTERIZATION

Original Research



Metal release profiles of NiTi and stainless steel orthodontic appliances: the influence of proteinaceous immersion media vs artificial saliva

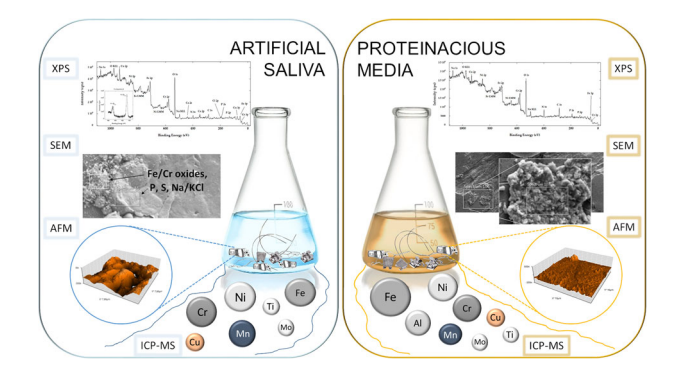
Mirna Petković Didović¹ · Koray Kara² · Ivana Jelovica Badovinac³ · Robert Peter³ · Željka Fiket⁴ · Iva Suman¹ · Tomasz Kowalkowski 60⁵ · Gordana Čanadi Jurešić¹

Received: 1 November 2024 / Accepted: 1 April 2025 © The Author(s) 2025

Abstract

When measured in vitro, the release of metal ions from orthodontic alloys is typically carried out in artificial saliva (AS), a medium with many advantages but lacking the biological complexity of natural human saliva. In this study, we measured ion release profiles from the complete orthodontic fixed appliance, comprising stainless steel and NiTi parts, in a proteinaceous media (yeast extract peptone dextrose, YPD) and compared it to AS. Two immersion models were used, differing in medium replenishment dynamics. To elucidate the metal release results, surface chemistry and topography were analysed using atomic force microscopy (AFM) followed by roughness analysis, and elemental analysis of the top micrometric and nanometric layer (SEM/EDX and XPS analyses). The results showed that proteinaceous media promoted the leaching of Fe, Cu, and Al while suppressing Ni and Cr. Ni²⁺ and Cr³⁺ ions were detected in the top layer on NiTi in AS, but not in YPD. A rough "wavy" surface layer was formed in AS, as opposed to smaller sharper entities formed in YPD. Cu(I) compounds on orthodontic bands were detected in both media. The replenishment of the media during immersion influenced the development of surface chemistry and ion leaching for both types of media, AS and YPD. The results obtained in this study are expected to provide a significant advancement over previous studies using artificial saliva (only).

Graphical Abstract



Deceased: Tomasz Kowalkowski.

Published online: 06 October 2025

- ☐ Gordana Čanadi Jurešić gordanacj@medri.uniri.hr
- Faculty of Medicine, Department of Medical Chemistry, Biochemistry and Clinical Chemistry, University of Rijeka, B. Branchetta 20, Rijeka, Croatia
- Graphene Application and Research Center, Izmir Katip Celebi University, Izmir, Turkey
- Faculty of Physics and Centre for Micro- and Nanosciences and Technologies, University of Rijeka, Radmile Matejčić 2, Rijeka, Croatia
- ⁴ Ruđer Bošković Institute, Bijenička 54, Zagreb, Croatia
- Faculty of Chemistry, Nicolaus Copernicus University, Gagarina 7 street, Torun, Poland



1 Introduction

Two main issues in current research on the suitability of orthodontic materials are passivation stability under the harsh conditions of the oral cavity and the release of harmful ions such as Cr³⁺ and Ni²⁺ [1–4]. Numerous studies have been conducted on these issues for typical orthodontic materials, and the vast majority of them used artificial saliva (AS) as the standard medium to mimic the oral environment [2, 5–8]. AS has many advantages as it is a standardised, controlled and easily accessible medium; however, it lacks the biological complexity of natural human saliva. In addition to a range of electrolytes – such as Na⁺, K⁺, Ca²⁺, Mg²⁺, Cl⁻, HCO₃⁻ and PO₄³⁻, which are present in a typical AS formula – natural saliva also contains a plethora of organic substances such as proteins (mucins, enzymes) and nitrogenous products [9]. In addition, AS does not contain microorganisms and does not take into account fluctuations caused by other factors such as diet [5]. On the other hand, yeast extract-peptone dextrose (YPD) medium contains peptides and other compounds similar to those found in natural saliva and mimic daily nutrition. Concretely, it contains a mixture of nucleotides, proteins, carbohydrates and trace elements (Y - yeast extract fraction), small peptides, lipids, vitamins and inorganic salts (P - peptone fraction) and glucose (D - dextrose). It has recently been shown that the yeast extract could reduce the corrosion rate of steel [10]. Also, Spark et al. found that peptide nutrients have an inhibitory effect on the corrosion of carbon steel [11]. However, the effect of YPD on the corrosion of metal parts of a fixed orthodontic appliance has not yet been investigated. In this study, we analysed how the YPD medium, affected the surface chemistry and topology of the actual orthodontic appliance parts and compared it to processes when only AS was used as a medium. Typical orthodontic alloys, stainless steel (SS) and NiTi were analysed. Due to the lowest detection limit, the ion release profiles over the period of one month were measured by inductively coupled plasma mass spectrometry. Even though the fixed appliance is typically worn for 1 - 2 years, the strongest changes in ion release are expected during this initial phase; moreover, the NiTi archwires (the main source of Ni²⁺ ions) are usually replaced every 1 - 2 months during the therapy [3]. Eliades et al. [12] pointed out that immersion studies aiming to mimic conditions in the oral cavity should include replenishment of the immersion medium rather than continuous immersion without replenishment, which is nonetheless still the predominant model. To the best of our knowledge, a direct comparison of the results obtained with these two types of immersion models has not been done. Therefore, in addition to analysing the differences in the ion release profiles of orthodontic parts in proteinaceous versus typical AS media, we also investigated two immersion models, which we termed "replenishment" (Model 1) and "continuous" (Model 2). To explain the differences in the release profiles, the surfaces of the orthodontic parts were analysed using atomic force microscopy (AFM), followed by a comprehensive surface roughness analysis, and SEM/EDX (energy dispersive X-ray) and X-ray photoelectron spectroscopy (XPS) for elemental analysis of the micrometric and nanometric surface layers, respectively. The results of this study are expected to provide a significant advancement over previous studies using artificial saliva (only).

2 Materials and methods

2.1 Orthodontic appliances

In each experiment, all parts constituting an entire orthodontic appliance were used: two archwires, twenty brackets, twenty ligatures, and four bands. The archwires (Rematitan[®] LITE ideal arches, φ 0.43 × 0.64 mm / 17 × 25, Dentaurum) were made of NiTi, an alloy of nickel and titanium (50 - 60% Ni + 40 - 50% Ti), while the bands (Dentaform, tooth 36, size 23 / Roth 22, Dentaurum), brackets (Equilibrium® 2, φ 0.56 ×0.76 mm / 22 ×30, Roth 22, Dentaurum) and ligatures (Remanium[®], short, soft, φ 0.25 mm / 10, Dentaurum) were made of SS. The detailed composition of all alloys, as well as all important material specifications, were listed in previously published results [13]. In short, although all parts of SS were made of austenitic steel, they differed in quality due to the specific requirements for each device. In the bands, Fe (65 - 69%)predominates, then Cr (17 - 19%), Ni (11 - 13%) and <2%Mn. The composition of the other two types of SS parts (brackets and ligatures) was similar - compared to the bands, they additionally contain only Mo (2.0 - 2.5%).

2.2 Experimental media

Two types of immersion media were used: 1) AS prepared by the Tani-Zucchi method (receipt in [13]), and 2) yeast complete growth media, YPD, i.e. a mixture of yeast extract (10 g/L), peptone (20 g/L), and dextrose (glucose, 20 g/L), both adjusted to pH 5.5. This pH value was chosen because YPD is used for the experiments with *Saccharomyces cerevisiae* W303, an auxotrophic mutant for Ura that is very sensitive to pH in the presence of metal ions in media and is able to grow only at certain pH values [14]. Also, this pH reflects the pH value found in patients with pure oral hygiene [15].

2.3 Preparation of orthodontic appliance eluates

We prepared all the samples (eluates in AS and YPD media) according to the current ISO standard (ISO 10993-5:2009), that describes test methods for evaluating the in vitro



cytotoxicity of medical devices. All parts were immersed in 28.0 mL of either AS or YPD media and autoclaved at 121 °C for 15 min (CertoClav, Austria) and then incubated under sterile conditions on a rotary shaker (37 °C, 100/min, Unimax 1010, Heidolph, Germany). The volume of the medium was calculated as 1 mL per cm of archwire (2 archwires, 14 cm each). Four samples were prepared for each type of medium. In Model 1 immersion, i.e. media replenishment, the total amount of medium was replenished after 3, 7, and 14 days. The same experiment was repeated, but without media replenishment, i.e. using continuous immersion, Model 2. The concentrations of metal ions were recorded on the 3rd, 7th, 14th and 28th day using an inductively coupled plasma mass spectrometer (ICP-MS).

2.4 Inductively coupled plasma mass spectrometry (ICP-MS)

1.0 mL of each eluate was mixed with 1.0 mL of concentrated HNO3 (Suprapure, Merck KGaA, Darmstadt, Germany) and heated to 80 °C (15 min). The eluate was then diluted to 10.0 mL with distilled water. ICP-MS system 2030 (Shimadzu, Kyoto, Japan) was used to analyze the prepared samples for 16 elements (Al, As, Be, Cd, Co, Cr, Cu, Fe, Mg, Mn, Mo, Ni, Pb, Sb, V, Zn). Polyatomic interferences were minimized by collision mode. Helium (6 mL/min) and argon (8 L/min) (Air Products, Toruń, Poland) served as a collision cell and plasma gas, respectively. The radiofrequency power was set to 1.2 kW and the collision cell voltage to $-21 \, \text{V}$. The limit of detection (LOD) and limit of quantification (LOQ) (expressed as $3 \times$ and 10 x the standard deviation) and other validation parameters of the analytical method were evaluated. Calibration curves were prepared by diluting the inorganic quality control standard (IQC-019, Ultra Scientific, North Kingstown, RI, USA) in 1% HNO₃ (Suprapure, Merck KGaA, Darmstadt, Germany). In addition, the 10-ppb platinum solution was continuously fed into the peristaltic pump as an internal standard via an additional tube. Both the dilution solutions and the internal standard were used to correct for matrix effects and signal drift. Correlation coefficients for all calibration curves were above 0.998 and LOQs were very low, but background equivalent concentrations (BEC) for cadmium, copper, lead, and zinc insisted that the working range was higher than a few µg/L because of the laboratory environment.

2.5 Cell culture

The hTERT-immortalized human gingival fibroblast (HGF) cell line (T0026) was purchased from ABM, Canada. Cells were grown in Dulbecco's Modified Eagle Medium (DMEM) supplemented with 10% fetal bovine serum

(FBS), and penicillin/streptomycin (all from Sigma-Aldrich, Steinheim, Germany) at 37 °C in 5% CO₂ in a humidified atmosphere. For the analysis, cells were seeded in 24-well plates (TPP, Trasadingen, Switzerland) until reaching 80% confluence and treated with previously prepared eluates (concentrated and reconstituted with growth media) for 24 h. Treatment with AS as an elution medium was used as a control. The cells were examined with the inverted microscope OCM 161 (KERN & SOHN GmbH), at a total magnification of 400x.

2.6 Atomic force microscopy (AFM)

Before imaging, samples were thoroughly cleaned (by successive rinsing with ethanol and deionized water, 3 min under ultrasound) to remove all surface contaminants, and then dried with a stream of N2. The cleaned samples were securely mounted to ensure that the samples were flat and fully adhered to the surface to avoid movement during scanning. A Nanosurf Easy Scan AFM configured for non-contact mode was used to minimise tip-sample interaction and potential damage. The noncontact mode with a silicon nitride tip was chosen to acquire topographic data. Before the measurements, the AFM system was calibrated using a standard calibration grid. The scan area was set to $10 \times 10 \mu m$, with scan rates adjusted to optimise resolution and minimize tip wear. The images were captured with sufficient resolution to recognise the necessary surface features. After acquisition, the images were processed with AFM software to reduce noise and improve contrast. Measurements of surface roughness, skewness, excess kurtosis, and other relevant morphological features were performed using the AFM software's analysis tools and Gwyddion (Czech Metrology Institute, Brno, Czech Republic), following the adapted procedure described by Skliar and Chernyshev [16]. All relevant parameters, including scan settings, tip specifications and environmental conditions, were carefully recorded to ensure reproducibility.

2.7 Scanning electron microscopy/energy dispersive X-ray (SEM/EDX) analysis

The surface morphology was studied with SEM (Jeol JSM-7800F, Japan). Three surface points for at least three identical appliance parts were tested, along with the minimum of six additional EDX examinations. In SEM analysis, the secondary electrons with an electron beam accelerating voltage of 10 kV and a working distance of 10 mm were collected. Representative samples were also tested with the EDX spectrometer (X-Max 80, Oxford Instruments, UK) in SEM with a beam acceleration voltage of 12 kV to study the elemental composition.



2.8 X-ray photoelectron spectroscopy (XPS) analysis

XPS was used to study the elemental composition of the top 10 nm of surfaces of the representative samples of archwires and bands. The photoemission spectra were recorded using a SPECS instrument under ultra-high vacuum conditions (the typical pressure in the analysis chamber was in the range of 10^{-7} Pa) with an excitation energy of 1486.74 eV (Al $K\alpha$ X-rays). The pass energy of the Phoibos 100 electron energy analyzer was set to 50 eV. The position of the C 1 s peak, adjusted to the binding energy of 284.5 eV, was used for the energy calibration.

2.9 Statistical analysis

For comparison of the eluted concentration of major metal ions from parts of the orthodontic appliance in immersion media, the analysis of variance (ANOVA) was used together with the Post hoc Tukey HSD test, p < 0.05 (using Statistica data analysis software system, version 13.4.04; Tibco Software Inc, Palo Alto, CA).

3 Results

3.1 ICP-MS results

3.1.1 Metal release profiles and relative amounts of released ions

Figure 1 shows the release profiles of the most abundant ions detected after 3, 7, 14, and 28 days of immersion in AS and YPD, with and without the replenishment of immersion medium after each measurement (Model 1 and Model 2, respectively). Ions detected in pure immersion liquids are also given. The comparison of the ion concentrations of Model 1 in AS and YPD (Fig. 1a and b) showed that the ion concentrations increased throughout the entire testing period both in AS and YPD, but with different profiles. Namely, the Fe concentration increased almost fourfold from day 3 to 28 (\sim 800 µg/L to \sim 3000 µg/L) in AS, whereas in YPD it reached \sim 3000 µg/L already after day 3 and then increased less steeply, reaching the final value of \sim 3900 µg/L. More leveled release profiles after higher initial values were also found for other ions in YPD, all except Co.

Additional observations can also be drawn from Fig. 1:
a) Fe concentrations were higher in YPD compared to AS, regardless of the immersion model used; b) Ni and Cr concentrations were lower in YPD compared to AS, regardless of the immersion model used; c) the majority of other ions leached less in YPD, except Cu and Al (besides already mentioned Fe); d) Fe was the most abundant ion in all cases, except when surpassed by Ni during continuous

immersion in AS; e) more than double the amount of iron was detected after continuous immersion in YPD compared to all other cases (note that Fig. 1d carries different scaling).

Regarding the influence of the immersion model change, the results indicated that this change 1) severly affected the outcome of the analysis and 2) had a distinctly different effect depending on the medium. Namely, continuous immersion in YPD caused a significant increase of Fe leaching and less severly of Ni leaching (Fig. 1b vs 1d), while a surge of Ni ions was recorded in AS (Fig. 1a vs 1c). Another prominent disparity was a change in release profiles characteristic only for this case (Fig. 1c), as the maximum of the release profiles of almost all ions was reached on day 14. Only the concentration of chromium began to decrease earlier, after day 7.

The results clearly indicate that both the choice of the medium and the choice of immersion protocol severly affected the mechanism of ion release, changing both the release profiles and the relative amounts of ions, as will be further discussed in the following.

3.1.2 Validation by changes in cell morphology

Before expanding the investigation, we sought to validate characteristic results given in Fig. 1c, due to its distinction from other cases. The variations in toxicity of orthodontic eluates taken after 3, 7, 14, and 28 days of immersion (Model 2) are illustrated in Fig. 2. Human gingival fibroblasts (HGF), the predominant cells of gingival connective tissue that play a key role in its maintenance, appeared spindle- or stellate-shaped and formed a confluent layer during normal growth (Fig. 2a) [17]. Treatment of HGF with AS did not lead to any change in cell growth and morphology changes (Fig. 2b). In the eluate-treated cells (Fig. 2c-f), the cells changed shape, shrank, and curled up, with a tendency to form filopodia (asterisks in the figures) that make contact with neighbouring cells. The formation of thin membranous bridges, so-called tunnelling nanotubes (TNTs), was observed [18], connecting cells over long distances (arrows). A certain number of cells changed their morphology and decreased their original number under the treatments. In addition, plaques appeared in the treated cells. Judging by the appearance of the cells, the loss of number, and the size of the plaques, the treatment with the eluate of 7 and 14 days seemed to have had the strongest toxic effect. Furthermore, the cells in the sample treated with the 28-day eluate appeared similar to the control cells, they were spindle-shaped and had fewer number of filopodia. This effect therefore confirmed the ion release results shown in Fig. 1c.

3.2 AFM surface morphology analysis

To elucidate the ion release profiles shown in Fig. 1, the surface of the orthodontic bands was analyzed by AFM. Out



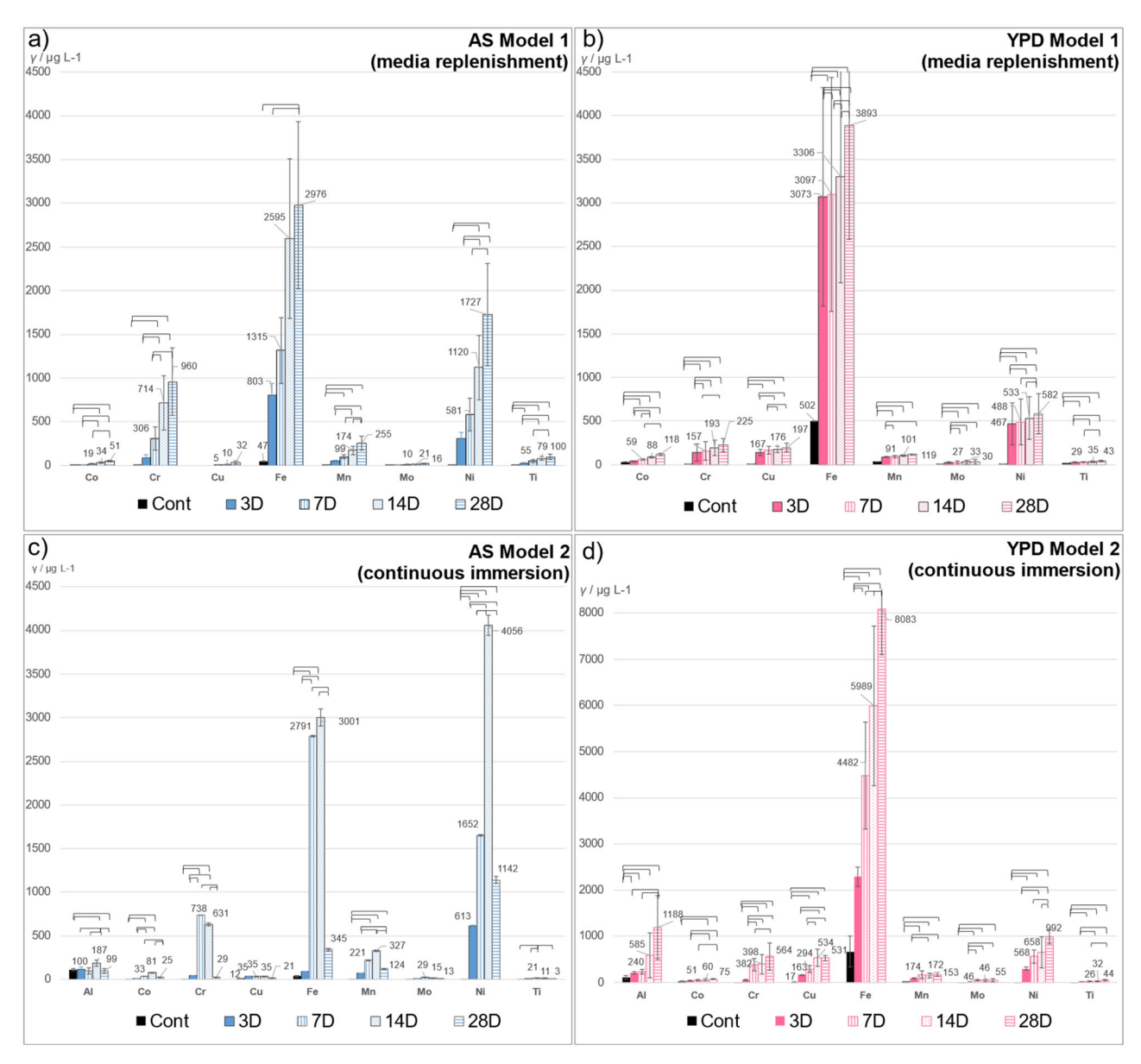


Fig. 1 The release profiles of the most abundant ions detected after 3, 7, 14 and 28 days of immersion in (a) artificial saliva (AS) using Model 1; **b** AS using model 2; **c** yeast dextrose medium (YPD) using model 1 and **d** YPD using Model 2. Model 1 and Model 2 denote immersion with and without replenishment of the immersion medium

after each measurement, respectively. The data are represented as mean \pm SD. The lines/connections indicate the metal ion concentrations that differ significantly (Anova, post hoc Tukey HSD test, p < 0.05)

of four types of orthodontic parts, the bands were chosen based on the previously obtained results [13] and an order of magnitude higher value of ion leaching, while continuous immersion was chosen due to the ion release profile results (Fig. 1c and d). Since the insufficient area of investigation (AOI) is an intrinsic disadvantage of AFM [19], care was taken to choose the most representative AFM micrographs. The surface of the bands was very heterogeneous [13], hence two micrographs are shown for each sample, best representing variations in topography within the same sample.

Due to surface heterogeneity, two images are shown for each sample.

The micrographs shown in Fig. 3 revealed different surface topographies depending on the medium, with noticeable preferred orientation of the peaks in some cases. To quantitatively describe the evolution of surface morphology during immersion in each medium and the differences between the two media, 3D amplitude parameters as well as spatial and hybrid roughness parameters were determined using the Gwyddion software. Figure 4a shows the root-mean-square surface roughness (S_q) , which



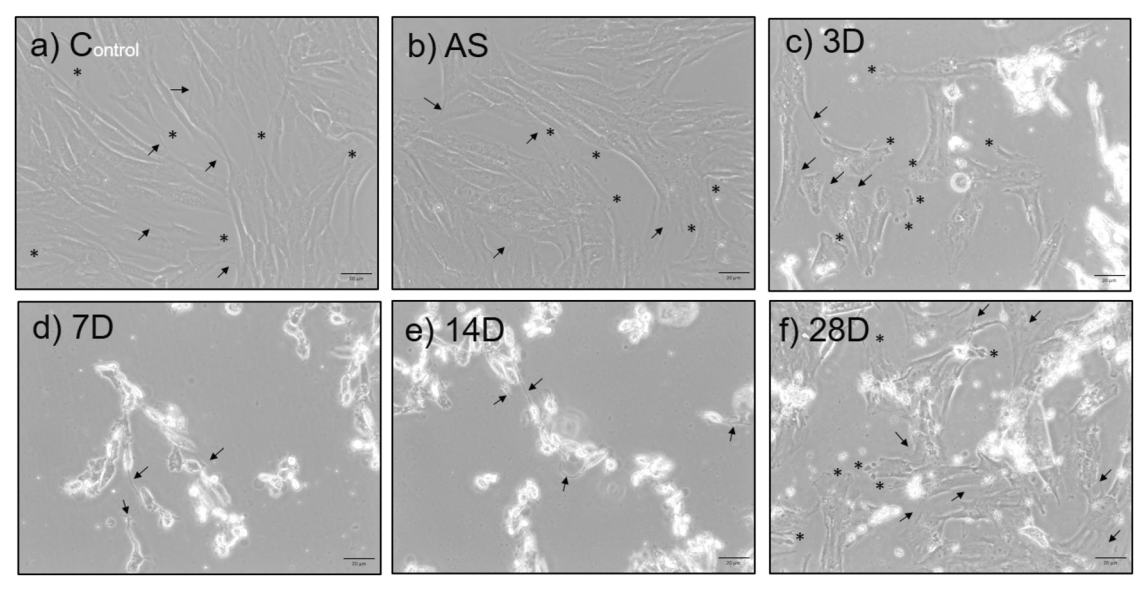


Fig. 2 Microscopic images of human gingival fibroblasts (a) untreated; b treated with artificial saliva; c-f treated with metal ion eluates, taken after 3, 7, 14 and 28 days of continuous immersion in AS

(magnification 400x). The asterisks indicate the filopodia formed, while the arrows indicate the tunnelling nanotubes

illustrates the general differences in roughness and the development of roughness during the immersion. For the sample immersed in AS, an increase in S_0 values from ~20 nm to >140 nm was measured, while it remained below 40 nm throughout the whole immersion time in YPD. The maximum peak height, S_2 , (Fig. 4b) was almost 1 µm in AS, while it remained below 500 nm in YPD. The decrease in S_7 was also measured after day 3 in YPD, followed by an increase with further immersion. The parameter S_{dq} (Fig. 4c) describes the developed interface. For the sample in AS, an increase in S_{dq} values was measured during immersion, reaching 0.6 on day 14, while the values in YPD remained twice as low throughout the immersion period. The skewness, S_{sk} , (Fig. 4d) provides information on the distribution of the heights of peaks and valleys, where $S_{sk} = 0$ means a symmetrical distribution (equal number of peaks and valleys), $S_{sk} < 0$ implies more valleys than peaks, and vice versa for $S_{\rm sk} > 0$. Before immersion, the surface was characterised by the predominance of valleys over peaks. For the sample in YPD, a continuous increase in S_{sk} values was measured, indicating the continuous appearance of new discrete peaks. In AS, the trend was less clear: the initial rise in the first days of immersion was followed by a decrease below zero. Kurtosis is another parameter related to the height distribution function. It has a value of 3 when the distribution is Gaussian (the peak heights are completely random). The excess kurtosis, S_{ku} , is used for easier comparison, as it describes how much the distribution deviates from the Gaussian distribution (i.e. from 3): higher values stand for a sharp distribution, i.e. a higher proportion of peaks with similar heights, and $S_{ku} = 0$ stands for complete randomness of the height distribution. For the sample in

YPD, the S_{ku} values increased during the immersion time, indicating that the peak heights became less random and more uniform. This is in contrast to the sample immersed in AS, where the values decreased to around 0 in later immersion phases, implying random peak heights. This agrees well with the changes in the skewness parameter and the visual evaluation of the AFM photomicrographs. Distinct smaller peaks in YPD had a preferred orientation in the early stages of immersion, as quantified by small S_{tr} parameter values (Fig. 4f). S_{tr} is a texture aspect ratio, with values below 0.5 (bold line in Fig. 4f) representing anisotropy of the surface patterns, while higher values reflect strong isotropy.

To gain insight into the chemical composition of the layer and the surface entities, SEM/EDX and XPS elemental analysis were performed and presented in the following. Note that the AFM results did not explain the excessive Ni concentrations in AS nor excessive Fe concentrations in YPD.

3.3 SEM/EDX and XPS analysis

3.3.1 NiTi archwires

Representative results of SEM analysis of NiTi wires after 28 days of continuous immersion in AS and YPD (Model 2) compared to as-received wire, are shown in Fig. 5a, while Fig. 5b shows the results of NiTi wires after 28 days and media replenishment (Model 1). The results of the elemental analysis were further processed so that only the key atoms were considered, and their relative ratios were calculated and shown in the figures.



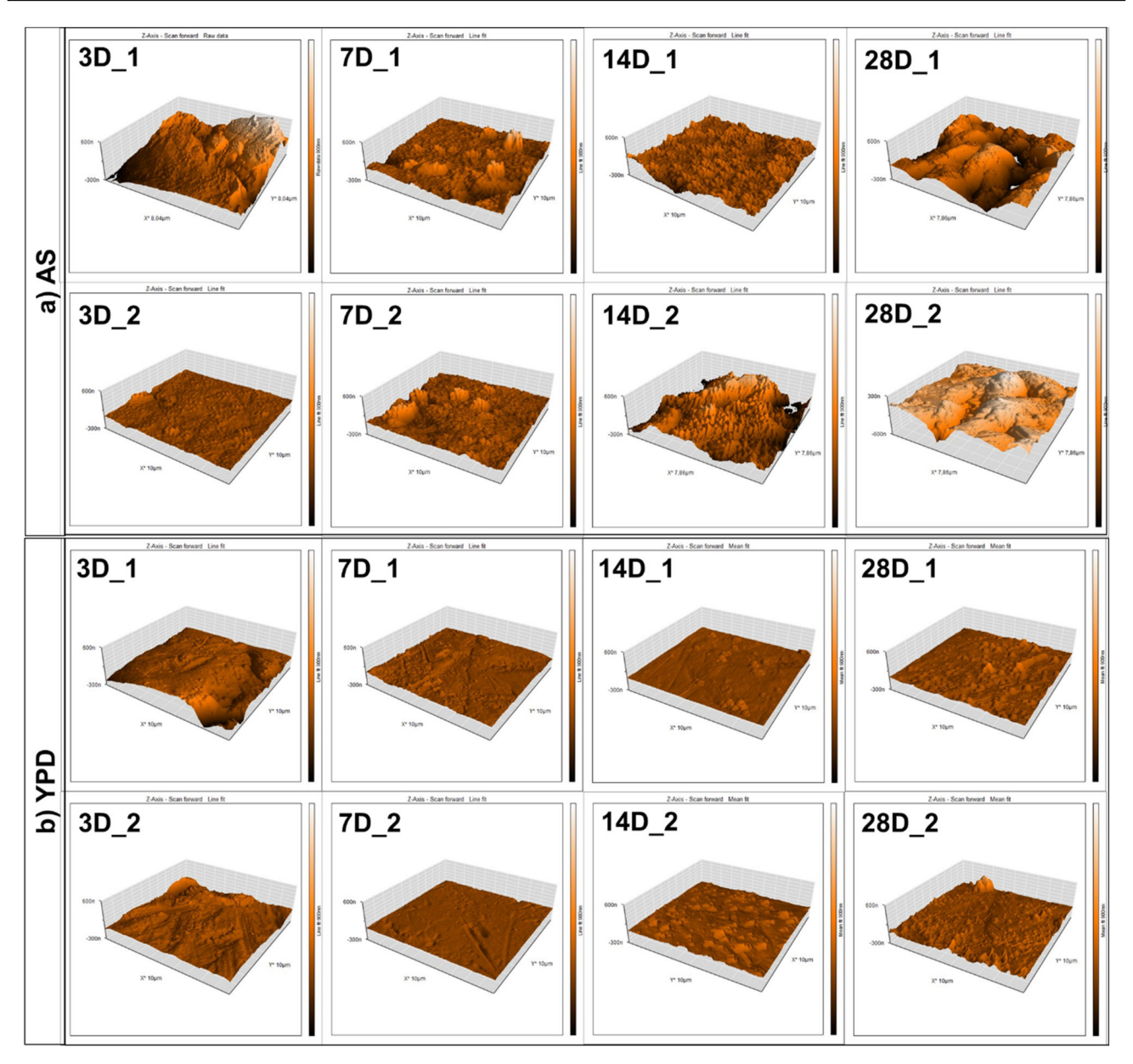


Fig. 3 Representative atomic force microscopy (AFM) photomicrographs of orthodontic band surface after immersion in (a) artificial saliva (AS) and b yeast complete medium (YPD) for 3, 7, 14, and 28 days

The samples in pristine state contained striations and crevices created by manufacturing [20], as described in detail in Petković Didović et al. [13]. Bundles of debris were observed within striations, but the surrounding surface was smooth and uniformly coloured and showed no signs of oxidation or corrosion (Fig. 5a). After 28 days in AS, the Ni:Ti ratio was close to the nominal ratio of the parent alloy. In terms of oxygen, two features were evident: systematically higher amounts of oxygen on smooth areas in AS compared to YPD (blue arrows), with negligible amounts in YPD; and markedly higher amounts of oxygen in crevices compared to smooth surfaces in both cases (red arrows).

Note that in addition to oxygen, the amount of Ti in the crevices also increased compared to Ni. Crystalline precipitates were dominated by Ca and K salts in both media – in clusters up to a few tens of micrometres in size – containing mainly Si and P as well as traces of Fe and Al.

XPS results (Fig. 6) revealed a Ni 2p peak with a binding energy of 854 eV, which can be ascribed to nickel ions in NiO or Ni(OH)₂ [21], only in the uppermost surface layer formed in AS, but not in YPD (blue/pink shadings, respectively). Also, almost double the amount of oxygen was found on YPD, confirming SEM/EDX results.



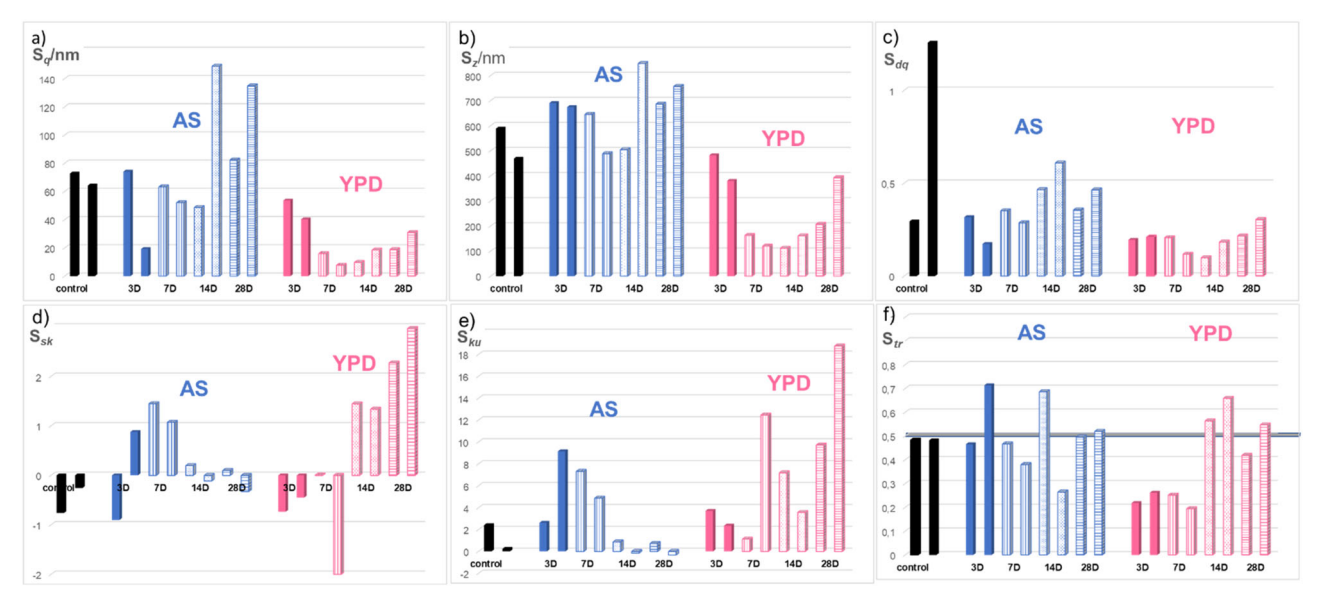


Fig. 4 Surface roughness parameters of the orthodontic bands during immersion in AS and YPD. **a** Root-mean-square surface roughness, S_q ; **b** maximum peak height, S_z ; **c** developed interfacial area, S_{dq} ; **d** skewness, S_{sk} ; **e** excess kurtosis, S_{ku} ; **f** texture aspect ratio, S_{tr}

3.3.2 SS bands

SEM/EDX results on bands during continuous immersion (Fig. 7a) showed, in general, higher amounts of oxygen and bundles of surface deposits in AS compared to YPD, thus confirming AFM results. The deposits were identified as mixed Fe and Cr oxides or locally as pure Fe₂O₃. Areas reflecting the nominal elemental ratio (parent alloy) were also found, typically on smooth parts, and were more frequent in YPD.

Replenishing the fluids during immersion rendered the band's surface richer in chromium oxide and other mixed deposits, and this was more pronounced in AS (Fig. 7b). Areas with nominal composition of the parent alloy were again present. By far the most dominant feature in YPD was a thick layer comprising Cu and S, found also on the band surface in AS.

XPS spectra were recorded to elucidate the chemical composition of observed deposits (Fig. 8). Cu 2p peak with a binding energy of ≈940 eV was expectedly present in the XPS spectra of bands in both AS and YPD. Zooming in on this peak revealed it consisted of Cu 2p_{3/2} at 934 eV and 2p_{1/2} at 953 eV. As for the other observed deposits, XPS results showed that Fe is present in the form of FeO (708.5 eV) and Fe₂O₃ (711.5 eV). Cr in the form of Cr₂O₃ (577.5 eV) and Ni as NiO or Ni(OH)₂ (854 eV) were found in both cases [21]. Besides those oxides, oxygen could be a part of Na/K/Ca H₂PO₄⁻, PO₄³⁻, and CO₃²⁻ [22–24]. Also, double amounts of C and N were found for YPD media, which indicates the presence of organic compounds: a N peak at 399 eV fits the N in the CN group, in the N-C bond

in amines, and in the N-C = O group [25]. P was present in both samples, likely in the form of PO_4^3 (134.5 eV) [22].

4 Discussion

4.1 ICP-MS results

4.1.1 Metal release profiles and relative amounts of released ions

The release profiles measured in the AS (Fig. 1a) showed that the concentrations of all ions in Model 1 increased continuously over the entire testing period. This was not the case for Model 2 (Fig. 1c), where most of the ions reached the maximum elution on day 14, which was followed by a prominent decrease. The exception was Cr, whose concentration began to decrease earlier, after day 7. The sudden drop in eluted concentrations after day 14 for most ions indicates the formation of a protective layer [26] that prevents further ion release. It is known that Cr ions are the main components of the protective layer on chromiumcontaining SS, which provides an explanation why the Cr concentration decreased earlier compared to the other ions as they were consumed in the formation of the passive layer. Surprisingly, the change from Model 1 to Model 2 in YPD (Fig. 1b and d) did not have the same effect on the release profiles as in AS (Fig. 1a and c): Concentrations of most ions in YPD increased throughout. This important result indicates that the nutrients in YPD influenced the formation of the protective layer. However, the change in immersion



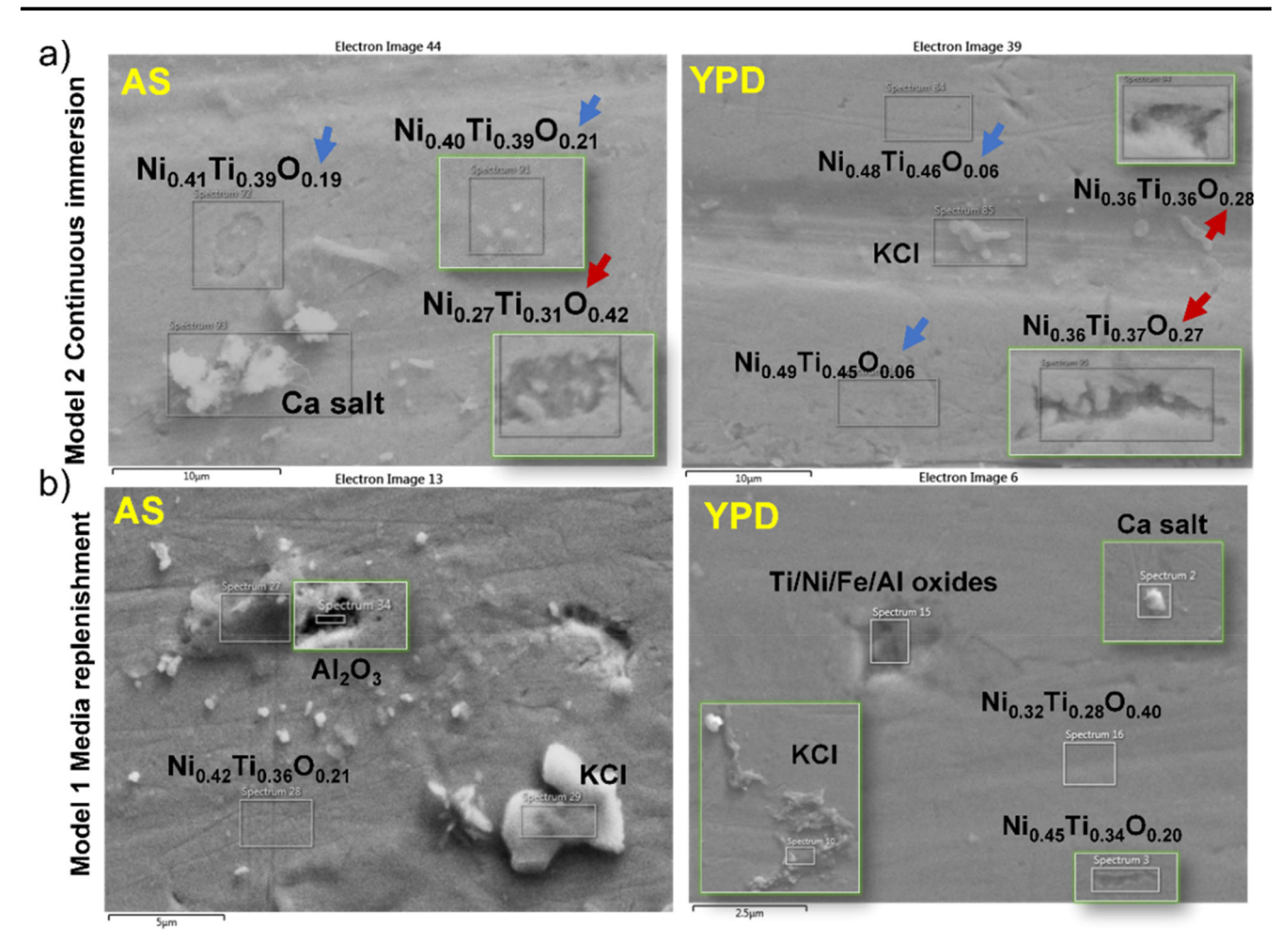


Fig. 5 SEM/EDX analyses of the orthodontic NiTi archwires after 28 days of immersion in AS and YPD (a) continuously (Model 2) and **b** with media replenishment (Model 1). All subsequently added parts

of the images are framed by green frames. Blue arrows stand for normal values, while red for markedly higher amounts of oxygen

models affected the release profiles in YPD to a certain extent and clearly influenced the amounts of released ions.

The ICP-MS results indicated that the ion release profiles were influenced by both the dynamics of media replenishment and the choice of medium. When the orthodontic appliance parts were continuously placed in the AS for 28 days, a protective layer appeared to form, which was sufficient to reduce leaching, while replenishment of the AS media resulted in continuous ion leaching. On the other hand, the protective layer either did not form or was not thick enough to reduce ion leaching in YPD media during the test period, regardless of the dynamics of media exchange.

4.2 AFM surface morphology analysis

The changes in surface roughness were more prominent during the immersion in AS compared to YPD, and different surface topographies developed depending on the media (Fig. 3). Prior to immersion, the surface in both media was characterised by the predominance of valleys over peaks. For the sample in YPD, a continuous increase in $S_{\rm sk}$ values was measured, indicating the continuous appearance of new discrete peaks. In AS, the trend was less clear: the initial rise in the first days of immersion was followed by a decrease below 0. This indicates that a thicker, rougher, "wavy" layer characterised by a similar number of peaks and valley, forms in later phases of immersion. It is also confirmed by the values of the excess kurtosis, S_{ku} (Fig. 4e). For the sample in YPD, the S_{ku} values increased during the immersion time, indicating that the peak heights became less random and more uniform. This agrees well with the changes in the skewness parameter and the visual evaluation of the AFM photomicrographs.

The AFM results showed different trajectories of the evolution of the surface topography during immersion in AS and YPD. The results pointed out the formation of a rough surface layer in the AS medium, in contrast to smaller, sharper entities that formed in YPD.



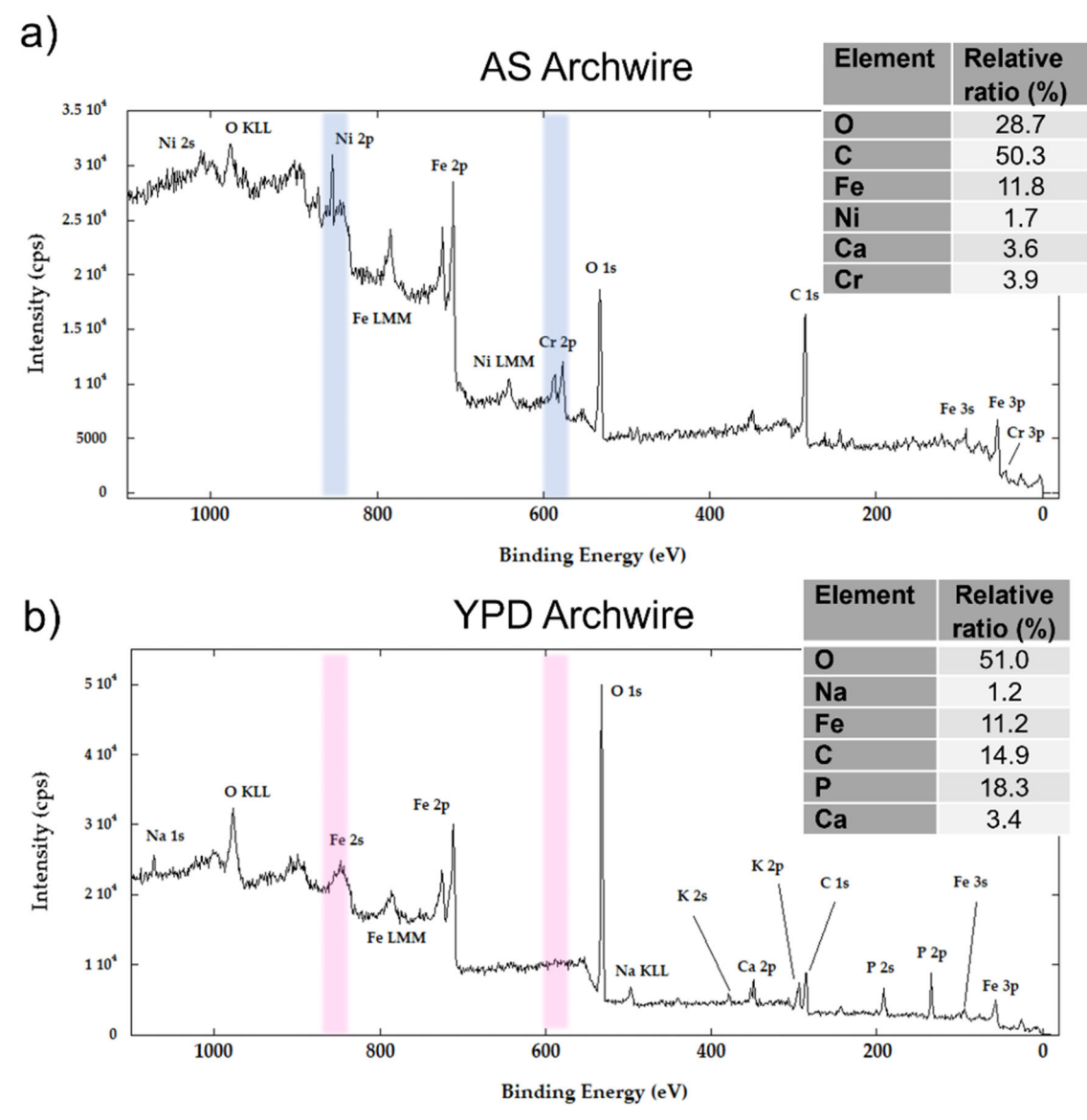


Fig. 6 XPS spectra of the top 10 nm of NiTi archwire surface after 28 days of immersion in AS (a) and YPD (b) and the elemental analysis. Blue and pink shadings emphasize the absence of Ni 2p peak in the uppermost layer in YPD

4.3 SEM/EDX and XPS analysis

4.3.1 NiTi archwires

Compared to XPS, the SEM/EDX technique allows elemental analysis of a thicker part of the surface (in the order of 1 μ m) and focuses on the material below the top layer [27, 28]. Despite its limitations – lower accuracy for lighter elements, accumulation of carbon on the surface [29–31] – it is advantageous because it gives an insight into the surface morphology of a larger AOI and thus allows easier detection of crystalline precipitates, defects and corrosion signs. Comparing obtained elemental compositions in this study (Fig. 5) with the results of Firstov et al. [20], where a

uniform oxide layer with composition Ni_{0.46}Ti_{0.31}O_{0.23} was established after oxidation of NiTi wires at 300 °C, it can be inferred that the oxide layer began to form during immersion in AS, but not in YPD, which is in accordance with the AFM results on bands (Fig. 3). The oxide layer in AS was not thick enough to exhibit its specific porous texture [32, 33]. Oxidation was more pronounced in the crevices, which is consistent with the well-known concept that surface defects can trap oxygen and thus promote oxidation [33, 34]. The increase in Ti content along with oxygen indicates that Ti is preferentially oxidised over Ni [33, 35], which is consistent with the known fact that TiO₂ is the most stable and abundant oxide formed on NiTi wires [26, 32, 35]. The results also confirmed that the sudden drop



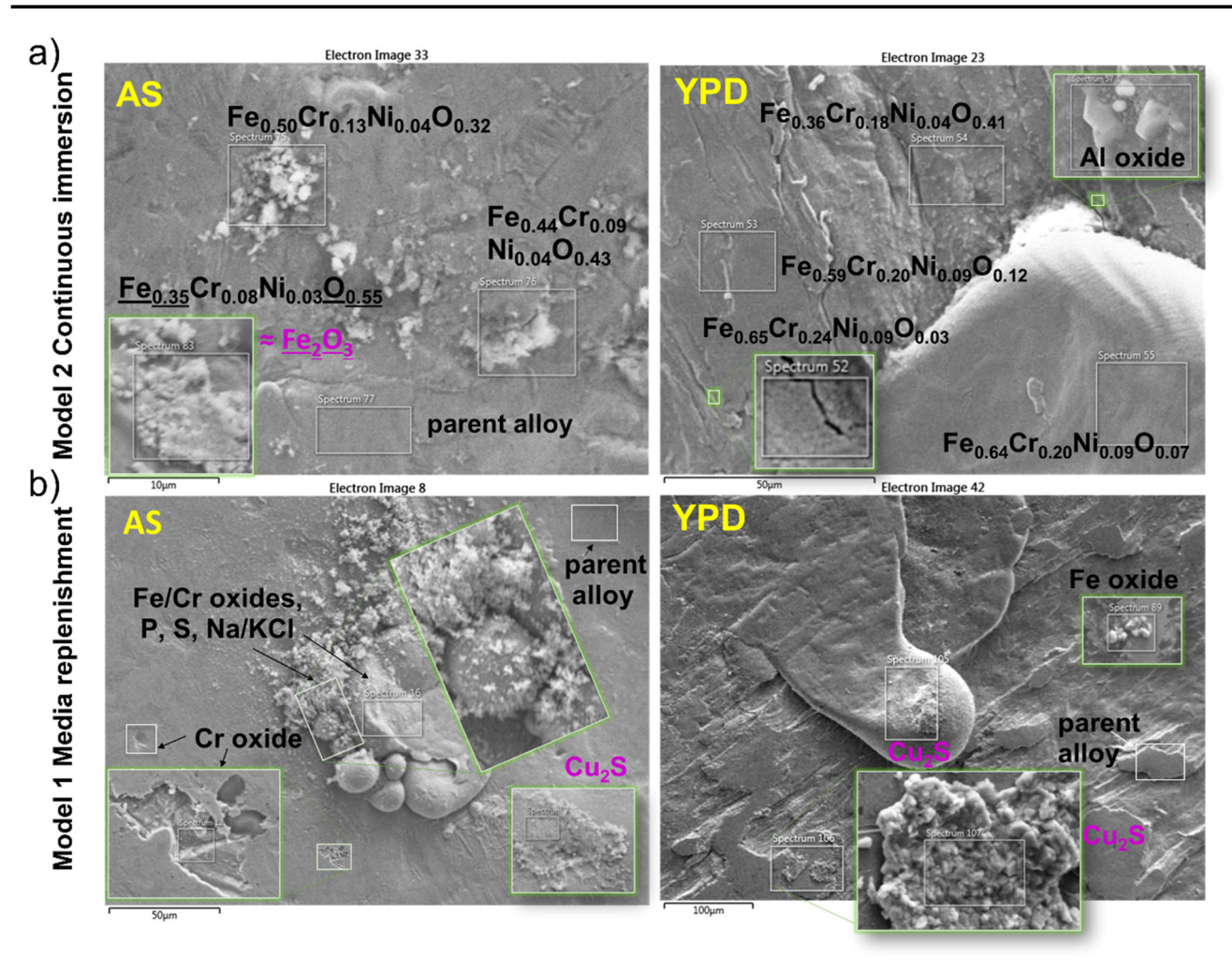


Fig. 7 SEM/EDX analyses of the orthodontic bands after 28 days of immersion in AS and YPD (a) continuously (Model 2) and (b) with media replenishment (Model 1). All subsequently added parts of the images are framed by green frames

in eluted Ni concentrations between the 14th and 28th day of immersion in AS was caused by a protective layer that did not form in YPD, where Ni concentrations continued to rise. Despite this sudden drop in Ni concentration in AS to ~1.1 mg/L, Ni concentrations in YPD did not exceed this value even at the end of the immersion period. The results indicated that Ni leaching in YPD was suppressed by a different mechanism. This simple situation, in which the compounds present in YPD appeared to inhibit the formation of a protective layer on NiTi within the first 28 days of continuous immersion, was not repeated when the medium was regularly replenished (Fig. 5b). Although the elemental composition in AS again indicated the presence of a thin oxide layer, the YPD immersion revealed a more heterogeneous NiTi surface, rich in large crystalline precipitates (~100 μm) and increased oxygen content. This may have been the cause of the suppressed leaching of Ni ions in YPD compared to AS. Note that the focus of this analysis was the Ni release (and not other ions), as we assumed that Ni was leached only from the NiTi wires (as the richest Ni source in the intraoral environment [34]) and not from the SS parts.

The XPS results provided an explanation for higher Ni concentrations in AS eluates compared to YPD: the evolution of surface chemistry during immersion in AS yielded Ni (in the form of NiO or Ni(OH)₂) in the uppermost 10 nm of the layer, first in contact with immersion fluid, while in YPD they remained in the deeper parts of the surface. Interestingly, Ti-oxides were not detected in the uppermost 10 nm (Ti 2p peaks from various Ti-oxides would be located around 460 eV). XPS results also showed higher amounts of crystalline precipitates in YPD, as seen on SEM micrographs, and confirmed them as K and Ca-P salts. Ca-P crystalline precipitates were found by Eliades et al. on the retrieved NiTi wire surface in an in vivo study [36]. Furthermore, XPS results showed that, both in AS and YPD, the NiTi surface contained Fe in similar amounts, in the form of FeO (708.5 eV) and Fe₂O₃ (711.5 eV). Cr in the form of Cr₂O₃ (577.5 eV) was found only in AS (blue/pink



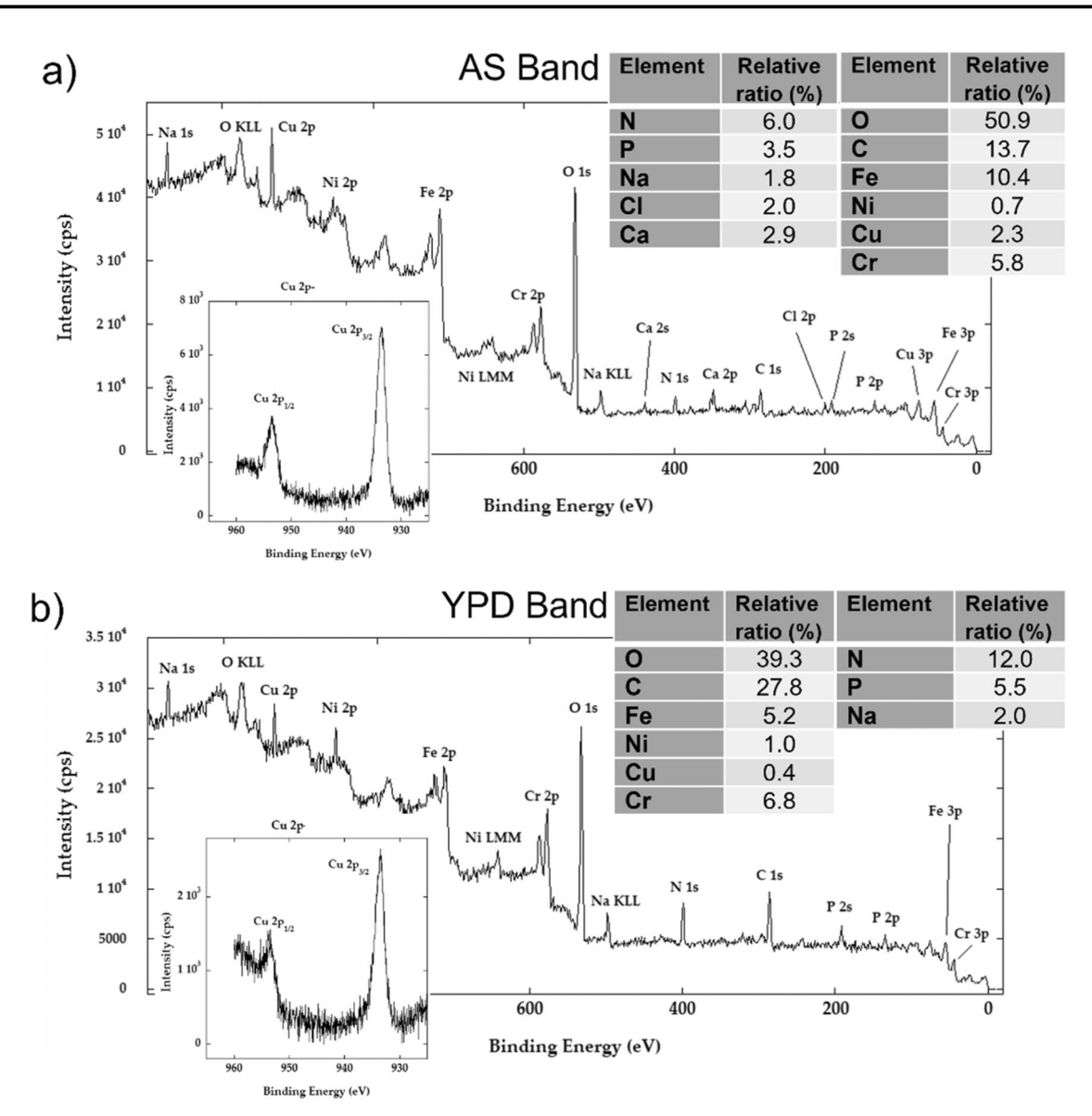


Fig. 8 XPS spectra of the bands after 28 days of immersion in AS (a) and YPD (b) and the elemental analysis. The addendum shows the "zoomedin" part around the Cu 2p peak. The absence of a "shake-up" peak at ~940 eV, characteristic of Cu(II), indicates the presence of Cu(I) compounds

highlights). Carbon 1 s peak, more pronounced in AS, was ascribed to adventitious carbon, i.e. surface contamination [35, 37, 38]. Fe and Cr are not relevant constituents of NiTi wires, hence those signals came from Fe- and Cr oxide precipitates.

The results indicated that two types of layers can be distinguished on the NiTi surface: the adsorption layer from precipitates formed from a combination of ions released from SS parts (Fe, Cr) and those contained in immersion fluids, and the oxygen layer formed from the oxidation of the parent material itself. Similar results were obtained with two types of NiTi archwires after 35 days of immersion (conditioning) in RPMI medium supplemented with amino acids and antibiotics [20]. The NiTi surface in continuous

immersion in YPD was the exception, as only in this case the oxide layer could not be detected.

4.3.2 SS bands

SEM/EDX results on bands indicates that the uniform oxide layer was not formed on bands during the first 4 weeks of immersion in either of the fluids, but the overall amount was larger in AS (Fig. 7). This difference seems to be sufficient to cause different ion release profiles measured by ICP-MS (Fig. 1c and d) and contributed to the Fe concentration surge in YPD. SEM micrographs did not reveal any signs of pitting corrosion, as a primary contestant for the cause of increased Fe leaching. Furthermore, deposits containing Al



Table 1 The summary of the key differences in ion release profiles and surface morphology of NiTi and stainless steel orthodontic appliances in artificial saliva (AS) and proteinaceous yeast extract peptone dextrose media (YPD)

| | AS | YPD |
|---------|--|---|
| ICPMS | dominance of Fe, Ni and Cr ions continuous immersion: prominent increase of the Ni concentration; suppression of the leaching of all ions after day 14 | suppression of Ni and Cr leaching continuous immersion: prominent increase of the Fe concentration; steady increase of all ions throughout the testing period |
| AFM | thicker, rough "wavy" layer S_q: 50-140 nm S_{ku} decreased with immersion time S_z > control and 500 nm S_{sk} changed with immersion time | $ \begin{tabular}{ll} \bullet & smaller & sharper & peaks \\ \bullet & S_q & < & control \\ \bullet & S_{ku} & increased & with immersion time \\ \bullet & S_z & < & control & and & 500 & nm \\ \bullet & S_{sk} & changed & with immersion & time \\ \end{tabular} $ |
| SEM/EDX | the formation of a thin oxide layer, initiating at crevices Ti is oxidized in preference to Ni Cr and Fe ions form part of the adsorption layer on bands | the protective layer had not formed more heterogeneous surface, large crystalline precipitates (mainly Ca-P salts) |
| XPS | NiO / Ni(OH)₂ and Cr₂O₃ detected in the uppermost layer on the NiTi archwires higher content of Cu-containing deposits on the band surface | \bullet NiO / Ni(OH) $_2$ and Cr_2O_3 not detected in the uppermost layer on the NiTi archwires |

were found in both cases, but more frequently in YPD, which explains the 10-fold increase in Al concentrations measured by ICP-MS. Cu and S were found in roughly equimolar amounts in YPD, suggesting that the crystals are copper(II) sulfide. The observed crystal morphology agreed with CuS crystals synthesized by other authors [39, 40]. However, it is well known that the crystal morphology varies depending on synthesis conditions, and Cu₂S crystals can be of similar morphology [41-45]. Perry and Taylor [44] studied XPS spectra of Cu₂S (chalcocite) and CuS (covellite) minerals and found almost identical Cu 2p peaks for both minerals. The underlying reason for this similarity is the fact that, although the stoichiometry would imply differently, in both cases the copper is in oxidation state +1[45]. While copper(I) compounds are diamagnetic, copper(II) compounds are paramagnetic, which is in XPS spectra manifested as a Cu(II) "shake-up" peak at ~940 eV and much broader copper(II) linewidths [44, 46-48]. As seen in both Fig. 8 addendums, this was not observed in results of this study. Also, Cu(0) and Cu(I) in copper(I) oxide have similar Cu 2p XPS patterns [48, 49]. Hence, the results indicated that a layer of Cu₂S was formed on the surface of the bands in both media, possibly accompanied by other Cu(I) compounds and elemental Cu. These Cucontaining deposits were observed on SEM micrographs on the band surface both in AS and YPD, but XPS results revealed 6-fold amounts of Cu in AS compared to YPD (2.3% vs 0.4%, respectively). A relatively large amounts of Cu are unusual since Cu is not listed in the nominal SS composition. As discussed in some papers, the likely source of Cu was the Cu-containing soldering alloy commonly used in orthodontics [13, 50]. The contact between more precious element with those found in SS alloy may trigger galvanic corrosion [51] and cause Cu release. This soldering

alloy is used in manufacturing SS parts, but not the NiTi parts, which explains the absence of Cu on NiTi surface.

5 Conclusions

The key findings of this study are summarized in Table 1.

The results of this study showed that ion release profiles and surface morphology of orthodontic alloys were affected by both the choice of the medium and the choice of immersion protocol. The interaction of organic molecules and metal ions in YPD enhanced the leaching of some ions (Fe, Cu, Al) while suppressing others (Ni, Cr). Nickel(II) ions in the form of NiO or Ni(OH)₂ and Cr(III) ions in the form of Cr₂O₃ were detected in the uppermost nanometric layer formed on the NiTi archwires in AS, but not in YPD. Ti-oxides were not detected in the uppermost layer in any case.

After one month of continuous immersion, a rough "wavy" surface layer was formed in AS, in contrast to smaller sharper entities of more uniform heights that formed in YPD. Surface roughness increased more prominently in AS than in YPD, reaching >140 nm, whereas it remained below 40 nm in YPD. The surface entities, predominantly mixed Fe and Cr oxides, adopted the preferred orientation at the onset of formation in YPD. The surface of the SS bands, but not the NiTi archwires, also contained Cu₂S and other Cu(I) deposits. The likely source of Cu was Cu-containing soldering alloy.

Immersion protocol conspicuously affected the outcome of ion leaching experiments. The evolution of the surface chemistry changed depending on whether or not immersion fluid replenishment was included in the protocol. Continuous immersion increased the differences between the two media and accelerated the formation of surface layers.



The average roughness R_a and other 2D roughness parameters were not sufficient descriptors of the topography of orthodontic alloys in the context of elucidating metal release profiles. 3D amplitude parameters as well as spatial and hybrid roughness parameters should be included to gain sufficient insight into the evolution of surface morphology during immersion.

Funding This research was funded by the Croatian Science Foundation within the framework of the Slovenian-Croatian bilateral project (IPS -2020-01-7418): "Determination of the occurrence, cause and harmful effects of oxidative stress caused by the use of fixed orthodontic appliances" and with the financial support of the University of Rijeka, projects by experienced scientists: Gordana Čanadi Jurešić (uniri-23-102) and Mirna Petković Didović (uniri-23-92).

Compliance with ethical standards

Conflict of interest The authors declare no competing interest.

Publisher's note Springer Nature remains neutral with regard to jurisdictional claims in published maps and institutional affiliations.

Open Access This article is licensed under a Creative Commons Attribution-NonCommercial-NoDerivatives 4.0 International License, which permits any non-commercial use, sharing, distribution and reproduction in any medium or format, as long as you give appropriate credit to the original author(s) and the source, provide a link to the Creative Commons licence, and indicate if you modified the licensed material. You do not have permission under this licence to share adapted material derived from this article or parts of it. The images or other third party material in this article are included in the article's Creative Commons licence, unless indicated otherwise in a credit line to the material. If material is not included in the article's Creative Commons licence and your intended use is not permitted by statutory regulation or exceeds the permitted use, you will need to obtain permission directly from the copyright holder. To view a copy of this licence, visit http://creativecommons.org/licenses/by-nc-nd/4.0/.

References

- Yue X, Zhang L, Hua Y, Wang J, Dong N, Li X, et al. Revealing the superior corrosion protection of the passive film on selective laser melted 316L SS in a phosphate-buffered saline solution. Appl Surf Sci. 2020;529:147170
- Barcelos AM, Luna AS, Ferreira NDA, Braga AVC, Lago DCBD, Senna LFD. Corrosion evaluation of orthodontic wires in artificial saliva solutions by using response surface methodology. Mater Res. 2012;16:50–64. http://www.scielo.br/scielo.php?script= sci_arttext&pid=S1516-14392013000100007&lng=en&tlng=en
- Petoumenou E, Arndt M, Keilig L, Reimann S, Hoederath H, Eliades T, et al. Nickel concentration in the saliva of patients with nickel-titanium orthodontic appliances. Am J Orthod Dentofacial Orthop. 2009;135:59–65. https://linkinghub.elsevier.com/retrieve/ pii/S0889540608007178
- Schmalz G, Arenholt-Bindslev D. Biocompatibility of dental materials. Berlin: Springer; 2009.
- Duffó GS, Castillo EQ. Development of an artificial saliva solution for studying the corrosion behavior of dental alloys. COR-ROSION. 2004;60:594–602. https://meridian.allenpress.com/

- corrosion/article/60/6/594/162259/Development-of-an-Artificial-Saliva-Solution-for
- Bobić Z, Kojić S, Stojanović GM, Terek V, Kovačević L, Terek P. Nanotopography evaluation of NiTi alloy exposed to artificial saliva and different mouthwashes. Materials. 2022;15:8705. https://www.mdpi.com/1996-1944/15/23/8705
- Łosiewicz B, Osak P, Górka-Kulikowska K, Goryczka T, Dworak M, Maszybrocka J, et al. Effect of artificial saliva modification on pitting corrosion and mechanical properties of the Remanium®-Type Orthodontic Archwire. Materials. 2023;16:6791. https://www.mdpi.com/1996-1944/16/20/6791
- Huang H. Surface characterizations and corrosion resistance of nickel-titanium orthodontic archwires in artificial saliva of various degrees of acidity. J Biomed Mater Res A. 2005;74A:629–39. https://onlinelibrary.wiley.com/doi/10.1002/jbm.a.30340
- Humphrey SP, Williamson RT. A review of saliva: Normal composition, flow, and function. J Prosthet Dent. 2001;85:162–9. https://linkinghub.elsevier.com/retrieve/pii/S0022391301540329
- Guan F, Pei Y, Duan J, Sand W, Zhang R, Zhai X, et al. Effect of yeast extract on microbiologically influenced corrosion of X70 pipeline steel by Desulfovibrio bizertensis SY-1. Bioelectrochemistry. 2024;157:108650. https://linkinghub.elsevier.com/ retrieve/pii/S1567539424000124
- Spark A, Cole I, Law D, Ward L. The effect of peptide based nutrients on the corrosion of carbon steel in an agar based system. Corros Sci. 2016;110:174–81. https://linkinghub.elsevier.com/ retrieve/pii/S0010938X16301834
- Eliades T, Athanasiou AE. In vivo aging of orthodontic alloys: implications for corrosion potential, nickel release, and biocompatibility. Angle Orthod. 2002;72:222–37.
- Petković Didović M, Jelovica Badovinac I, Fiket Ž, Žigon J, Rinčić Mlinarić M, Čanadi Jurešić G. Cytotoxicity of metal ions released from NiTi and stainless steel orthodontic appliances, part 1: surface morphology and ion release variations. Materials. 2023;16:4156.
- Pearce DA, Sherman F. Toxicity of copper, cobalt, and nickel salts is dependent on histidine metabolism in the YeastSaccharomyces cerevisiae. J Bacteriol. 1999;181:4774–9.
- Ferrer MD, Pérez S, Lopez AL, Sanz JL, Melo M, Llena C, et al. Evaluation of clinical, biochemical and microbiological markers related to dental caries. Int J Environ Res Public Health. 2021;18:6049.
- Skliar M, Chernyshev VS. Imaging of extracellular vesicles by atomic force microscopy. J Vis Exp. 2019;59254. https://app.jove. com/t/59254
- Lendahl U, Muhl L, Betsholtz C. Identification, discrimination and heterogeneity of fibroblasts. Nat Commun. 2022;13:3409. https://www.nature.com/articles/s41467-022-30633-9
- Gerdes H-H, Rustom A, Wang X. Tunneling nanotubes, an emerging intercellular communication route in development. Mech Dev. 2013;130:381–7. https://linkinghub.elsevier.com/ retrieve/pii/S0925477312001177
- Singh K, Paliwal N, Kasamias K. Surface roughness characterization using representative elementary area (REA) analysis. Sci Rep. 2024;14:1785. https://www.nature.com/articles/s41598-024-52329-4
- Firstov GS, Vitchev RG, Kumar H, Blanpain B, Van Humbeeck J. Surface oxidation of NiTi shape memory alloy. Biomaterials. 2002;23:4863–71
- Biesinger MC, Payne BP, Lau LWM, Gerson A, Smart RStC. Xray photoelectron spectroscopic chemical state quantification of mixed nickel metal, oxide and hydroxide systems. Surf Interface Anal. 2009;41:324–32.
- Sherwood PMA. Introduction to studies of phosphorus-oxygen compounds by XPS. Surf Sci Spectra. 2002;9:62–6.



- Demri B, Muster D. XPS study of some calcium compounds. J Mater Process Technol. 1995;55:311–4.
- Ni M, Ratner BD. Differentiating calcium carbonate polymorphs by surface analysis techniques—an XPS and TOF-SIMS study. Surf Interface Anal. 2008;40:1356–61.
- Vincent B The International XPS Database [Internet]. https://xpsdatabase.net/nitrogen-n-z7-nitrogen-compounds/
- House K, Sernetz F, Dymock D, Sandy JR, Ireland AJ. Corrosion of orthodontic appliances—should we care? Am J Orthod Dentofacial Orthop. 2008;133:584–92. https://linkinghub.elsevier. com/retrieve/pii/S0889540607009407
- Puttichaem C, Souza GP, Ruthe KC, Chainok K. Characterization of ultra-thin diamond-like carbon films by SEM/EDX. Coatings. 2021;11:729. https://www.mdpi.com/2079-6412/11/6/729
- Kumari K, Banerjee S, Chini TK, Ray NR. Preparation of diamond like carbon thin film on stainless steel and its SEM characterization. Bull Mater Sci. 2009;32:563–7. http://link.springer.com/10.1007/s12034-009-0085-x
- Hugenschmidt M, Adrion K, Marx A, Müller E, Gerthsen D. Electron-Beam-Induced Carbon Contamination in STEM-in-SEM: Quantification and Mitigation. Microsc Microanal. 2023;29:219–34. https://academic.oup.com/mam/article/29/1/219/6927139
- Farr NTH, Hughes GM, Rodenburg C. Monitoring carbon in electron and ion beam deposition within FIB-SEM. Materials. 2021;14:3034. https://www.mdpi.com/1996-1944/14/11/3034
- Carroll WM, Kelly MJ. Corrosion behavior of nitinol wires in body fluid environments. J Biomed Mater Res A. 2003;67A:1123–30. https://onlinelibrary.wiley.com/doi/10.1002/ jbm.a.10099
- Mahmud A, Wu Z, Zhang J, Liu Y, Yang H. Surface oxidation of NiTi and its effects on thermal and mechanical properties. Intermetallics. 2018;103:52–62. https://linkinghub.elsevier.com/ retrieve/pii/S0966979518307398
- Lafata MA, Rettberg LH, He MY, Pollock TM. Oxidation-assisted crack growth in single-crystal superalloys during fatigue with compressive holds. Metall Mater Trans A. 2018;49:105–16. https://link.springer.com/10.1007/s11661-017-4392-3
- Chan C, Trigwell M, Duerig S. T. Oxidation of an NiTi alloy. Surf Interface Anal. 1990;15:349–54. https://analyticalsciencejournals. onlinelibrary.wiley.com/doi/10.1002/sia.740150602
- Plant S, Grant D, Leach L. Behaviour of human endothelial cells on surface modified NiTi alloy. Biomaterials. 2005;26:5359

 –67.
- 36. Eliades T. Surface characterization of retrieved NiTi orthodontic archwires. Eur J Orthod. 2000;22:317–26.
- Grey LH, Nie H-Y, Biesinger MC. Defining the nature of adventitious carbon and improving its merit as a charge correction reference for XPS. Appl Surf Sci. 2024;653:159319.
- 38. Miller DJ, Biesinger MC, McIntyre NS. Interactions of CO 2 and CO at fractional atmosphere pressures with iron and iron oxide

- surfaces: one possible mechanism for surface contamination? Surf Interface Anal. 2002;33:299–305.
- Zhou X, Soldat AC, Lind C. Phase selective synthesis of copper sulfides by non-hydrolytic sol-gel methods. RSC Adv. 2014;4:717–26. https://xlink.rsc.org/?DOI=C3RA45053H
- Zou J, Zhang J, Zhang B, Zhao P, Huang K. Low-temperature synthesis of copper sulfide nano-crystals of novel morphologies by hydrothermal process. Mater Lett. 2007;61:5029–32. https:// linkinghub.elsevier.com/retrieve/pii/S0167577X07003515
- Johnson AL, Hill MS, Kociok-Köhn G, Molloy KC, Sudlow AL. The first crystallographically-characterised Cu(II) xanthate. Inorg Chem Commun. 2014;49:8–11. https://linkinghub.elsevier.com/ retrieve/pii/S1387700314003864
- Mousavi-Kamazani M, Salavati-Niasari M, Sadeghinia M. Synthesis and characterization of Cu2S nanostructures via cyclic microwave radiation. Superlattices Microstruct. 2013;63:248–57.
- 43. Yu Y, Yang D, Li J, Zhang M, Luo H, Liang Q, et al. A flash vacuum-induced reaction in preparing high performance thermoelectric Cu ₂ S. Adv Funct Mater. 2022;32:2107284. https://onlinelibrary.wiley.com/doi/10.1002/adfm.202107284
- Perry DL, Taylor JA. X-ray photoelectron and Auger spectroscopic studies of Cu2S and CuS. J Mater Sci Lett. 1986;5:384–6.
- Goh SW, Buckley AN, Lamb RN. Copper(II) sulfide? Miner Eng. 2006;19:204–8. https://linkinghub.elsevier.com/retrieve/pii/ S0892687505003018
- Mondal P, Sinha A, Salam N, Roy AS, Jana NR, Islam SM. Enhanced catalytic performance by copper nanoparticle–graphene based composite. RSC Adv. 2013;3:5615.
- 47. Tirado J, Roldán-Carmona C, Muñoz-Guerrero FA, Bonilla-Arboleda G, Ralaiarisoa M, Grancini G, et al. Copper sulfide nanoparticles as hole-transporting-material in a fully-inorganic blocking layers n-i-p perovskite solar cells: Application and working insights. Appl Surf Sci. 2019;478:607–14.
- 48. Biesinger MC, Hart BR, Polack R, Kobe BA. Smart RStC. Analysis of mineral surface chemistry in flotation separation using imaging XPS. Miner Eng. 2007;20:152–62. https://linkinghub. elsevier.com/retrieve/pii/S0892687506002093
- Raja M, Subha J, Ali FB, Ryu SH. Synthesis of copper nanoparticles by electroreduction process. Mater Manuf Process. 2008;23:782–5.
- Wendl B, Wiltsche H, Lankmayr E, Winsauer H, Walter A, Muchitsch A, et al. Metal release profiles of orthodontic bands, brackets, and wires: an in vitro study. J Orofac Orthop Fortschritte Kieferorthopädie. 2017;78:494–503.
- Eliades T, Zinelis S, Papadopoulos MA, Eliades G, Athanasiou AE. Nickel content of as-received and retrieved NiTi and stainless steel archwires: assessing the nickel release hypothesis. Angle Orthod. 2004;74:151–4.

